The EMBO Journal Vol. 21 No. 7 pp. 1661–1672, 2002

Essential role of endophilin A in synaptic vesicle budding at the *Drosophila* neuromuscular junction

Antoine Guichet[1,2], Tanja Wucherpfennig[3], Veronica Dudu[3], Sylvain Etter[4], Michaela Wilsch-Bräuniger[3], Andrea Hellwig[5], Marcos González-Gaitán[3], Wieland B.Huttner[3,6] and Anne A.Schmidt[4,6]

[1]Laboratory of Developmental Biology, Institut Jacques Monod, 2 place Jussieu, F-75251 Paris Cedex 05, [4]Institute of Biophysical Chemistry, UPR CNRS 1929, 13 rue Pierre et Marie Curie, F-75005 Paris, France, [2]Institute for Developmental Biology, University of Cologne, Gyrhofstrasse 17, D-50923 Cologne, [3]Max Planck Institute of Molecular Cell Biology and Genetics, Pfotenhauerstrasse 108, D-01307 Dresden and [5]Department of Neurobiology, Interdisciplinary Center of Neuroscience, University of Heidelberg, Im Neuenheimer Feld 364, D-69120 Heidelberg, Germany

[6]Corresponding authors
e-mail: huttner@mpi-cbg.de or anne.schmidt@ibpc.fr

We characterized *Drosophila* endophilin A (D-endoA), and generated and analysed D-endoA mutants. Like its mammalian homologue, D-endoA exhibits lysophosphatidic acid acyl transferase activity and contains a functional SH3 domain. D-endoA is recruited to the sites of endocytosis, as revealed by immunocytochemistry of the neuromuscular junction (NMJ) of mutant L3 larvae carrying the temperature-sensitive allele of dynamin, *shibire*. D-endoA null mutants show severe defects in motility and die at the early L2 larval stage. Mutants with reduced D-endoA levels exhibit a range of defects of synaptic vesicle endocytosis, as observed at L3 larvae NMJs using FM1-43 uptake and electron microscopy. NMJs with an almost complete loss of synaptic vesicles did not show an accumulation of intermediates of the budding process, whereas NMJs with only slightly reduced levels of synaptic vesicles showed a striking increase in early-stage, but not late-stage, budding intermediates at the plasma membrane. Together with results of previous studies, these observations indicate that endophilin A is essential for synaptic vesicle endocytosis, being required from the onset of budding until fission.

Keywords: clathrin/endophilin/membrane curvature/membrane lipids/synaptic vesicles

Introduction

The recycling of the synaptic vesicle (SV) membrane from the presynaptic plasma membrane is one of the paradigms of clathrin-mediated endocytosis. Like the formation of any vesicular carrier, formation of a clathrin-coated vesicle comprises two principal types of membrane dynamics, i.e. membrane budding and fission. The budding process is characterized by an increase in the curvature of the membrane and/or the amount of curved membrane. Although in essence continuous, the budding process is often viewed in two phases: (i) the early stages in which planar membrane becomes a hemispherical ('shallow') pit and; (ii) the late stages in which the hemispherical pit becomes a near-spherical ('deeply invaginated' or 'constricted') pit. The latter then undergoes fission at the neck to yield an endocytic vesicle.

The core of the protein machineries involved are the clathrin coat, which has a key role in the membrane budding process, and the GTPase dynamin, which is required for the fission step (Sever *et al*., 2000). Several additional proteins have been reported to interact with the clathrin coat and/or dynamin and have been implicated in the endocytic process (Sever *et al*., 2000; Slepnev and De Camilli, 2000). These include the endophilins, a protein family originally described in mammals, and, in the case of SV endocytosis, specifically endophilin A1 (Huttner and Schmidt, 2000), whose neurone-specific expression matches that of dynamin 1 (Ringstad *et al*., 1997). Via its C-terminal src homology 3 (SH3) domain, endophilin A1 physically interacts with proline-rich domains (PRDs) of (i) dynamin (Ringstad *et al*., 1997), (ii) amphiphysin (Micheva *et al*., 1997), which in turn interacts with the clathrin coat (Slepnev and De Camilli, 2000), and (iii) synaptojanin (Ringstad *et al*., 1997), a poly-phosphoinositide phosphatase implicated in uncoating (Slepnev and De Camilli, 2000).

An intriguing property of endophilin A1, which resides in its conserved N-terminal domain [referred to as the LBM (lipid binding and modifying) domain], is its ability to interact directly with lipids; specifically, to bind lysophosphatidic acid (LPA) and acyl-coenzyme A and to condense them to phosphatidic acid (PA) (Schmidt *et al*., 1999). Using a cell-free system derived from PC12 cells, endophilin A1 has been shown to be essential for the formation of synaptic-like microvesicles (SLMVs) from the plasma membrane, and its lipid binding and modifying capacity, which has been proposed to induce changes in membrane curvature, has been implicated in this process (Schmidt and Huttner, 1998; Schmidt *et al*., 1999; Huttner and Schmidt, 2000). Consistent with this, the binding of the LBM domain of endophilin A1 to liposomes has been shown very recently to result in the formation of narrow tubules (Farsad *et al*., 2001). These observations raise the questions as to how exactly endophilin A1 operates in SV membrane recycling from the plasmalemma, i.e. at which specific step(s) within the cascade of budding and fission it acts, and what effects arise from its capacity to bind and modify the above lipids.

One of the models of endophilin A1 action attributes significance to (i) its interaction with dynamin; (ii) the different shapes of LPA and PA; and (iii) the consideration that an endophilin A1-mediated conversion of membrane LPA to PA should make the curvature of the cytoplasmic

leaflet more negative (Schmidt *et al*., 1999; Huttner and Schmidt, 2000). Specifically, endophilin A1 has been proposed to act, in concert with dynamin, at the late stages of clathrin-mediated SV endocytosis, which are characterized by major changes in membrane curvature, being involved in the formation of a deeply invaginated pit, the constriction of the neck and fission (Huttner and Schmidt, 2000). Indeed, consistent with a role for endophilin A1 in the formation of a deeply invaginated pit, microinjection into the lamprey giant synapse of an antibody against the SH3 domain of endophilin, which results in the depletion of SVs, causes the accumulation of shallow coated pits at the plasma membrane (Ringstad *et al*., 1999), indicative of membrane budding proceeding up to, but not beyond, the hemispherical stage. There is also evidence for a role for endophilin A1 in even later stages of endocytosis, i.e. fission. Addition of the SH3 domain of endophilin A1 to a cell-free system blocks formation of endocytic vesicles at a step after formation of deeply invaginated coated pits (Simpson *et al*., 1999). Furthermore, microinjection into the lamprey giant synapse of the SH3 domain of endophilin, which also results in the depletion of SVs, causes the accumulation of deeply invaginated coated pits (Gad *et al*., 2000). Hence, with these types of interference, membrane budding proceeds beyond the hemispherical stage up to the near-spherical stage, with only the remaining fission step being blocked. Together, these studies establish that interfering with the SH3 domain of endophilin A1 blocks the transition from the early stages to, and the progression through, the late stages of clathrin-mediated endocytosis.

However, interfering with its SH3 domain does not necessarily reveal all aspects of endophilin A1 function in SV endocytosis. This may require studying synapses in which the presence of endophilin A1 has been abolished or its level drastically reduced. In the present study, we have extended our previous *in vitro* work (Schmidt and Huttner, 1998; Schmidt *et al*., 1999), in which the consequence of the virtual absence of endophilin A1 on SLMV endocytosis from the plasma membrane was studied in a cell-free system, to real synapses *in vivo*, studying the neuromuscular junction (NMJ) of *Drosophila* mutants lacking endophilin.

Results

D-endoA exhibits lysophosphatidic acid acyl transferase activity and contains a functional SH3 domain

We found two endophilins in the *Drosophila* genome, both of which have the same domain organization as mammalian endophilins, endophilin A (D-endoA) and endophilin B (D-endoB) (Figure 1) (Huttner and Schmidt, 2000) (for details see Supplementary data available at *The EMBO Journal* Online).

Since mammalian endophilin A1 exhibits lysophosphatidic acid acyl transferase (LPAAT) activity (Schmidt *et al*., 1999), we investigated whether this is also the case for D-endoA. Recombinant D-endoA, expressed in bacteria as a GST fusion protein and purified by glutathione affinity chromatography, was indeed able to condense LPA and acyl-CoA to PA (Figure 2A). The LPAAT activity of D-endoA was in the range previously reported for mammalian endophilin A1 (Schmidt *et al*., 1999) and much greater than that of a virtually inactive GST mouse endophilin A1 fusion protein used as control (Figure 2A).

A characteristic feature of the SH3 domain of mammalian endophilin A1 is its selective binding to poly(L-proline)–Sepharose (Schmidt *et al*., 1999). To investigate whether the putative SH3 domain of D-endoA also exhibits this property, D-endoA and, for comparison, mouse endophilin A1 were expressed in bacteria and a high-speed supernatant of the bacterial lysate was incubated with poly(L-proline)–Sepharose (Schmidt *et al*., 1999). Indeed, D-endoA, like mouse endophilin A1, specifically bound to poly(L-proline)–Sepharose, as confirmed by immunoblotting (Figure 2B).

These data show that both intrinsic LPAAT activity and the presence of a functional SH3 domain are features conserved between *Drosophila* and mammalian endophilins A.

D-endoA is expressed specifically in the central nervous system, localized in presynaptic terminals and recruited to sites of endocytosis

The expression pattern of D-endoA in various tissues was investigated by *in situ* hybridization of *Drosophila* embryos and by immunofluorescence of *Drosophila* larvae (Figure 3). In stage 17 embryos, the D-endoA mRNA showed a high level of expression in the central nervous system (CNS), both in the brain and in the ventral cord (Figure 3A). In the peripheral nervous system, D-endoA mRNA expression was detectable in the Bolwig organs (Figure 3A, arrow). The D-endoA mRNA became detectable early in the development of the CNS, as shown for the stage 11 embryo (Figure 3A).

To investigate the expression of the D-endoA protein, we raised a rabbit antiserum against a synthetic peptide corresponding to the C-terminal end of the LBM domain of D-endoA (see Figure 1A) whose sequence is specific for D-endoA versus D-endoB (see Figure 1B), and purified the antibody by affinity chromatography using the same peptide. Double immunofluorescence of flat body preparations of L3 larvae using this affinity-purified antibody and a monoclonal antibody against fasciclin II, a protein localized to synaptic membranes, revealed the specific localization of D-endoA in synapses, as shown for the NMJ in Figure 3B.

Within synapses, D-endoA was found presynaptically, in the regions of the cytoplasm containing SVs (Figure 4B), as revealed by its co-localization with cysteine string protein (CSP, Figure 4A), a marker of SVs. This localization of D-endoA within the presynaptic terminals (Figure 4K) was distinct from that of dynamin, which showed a pattern characteristic of recruitment to sites of endocytosis (Estes *et al*., 1996; González-Gaitán and Jäckle, 1997), as observed in NMJs of *shibire* L3 larvae kept at permissive temperature without stimulation (Figure 4I). Upon shift to restrictive temperature and depolarization to induce the SV exocytosis–endocytosis cycle, the pattern of dynamin staining did not change significantly (Figure 4J) (González-Gaitán and Jäckle, 1997), whereas D-endoA was now concentrated at sites of endocytosis (Figure 4L).

These results indicate that D-endoA (i) is expressed specifically in neurones; (ii) is localized in presynaptic

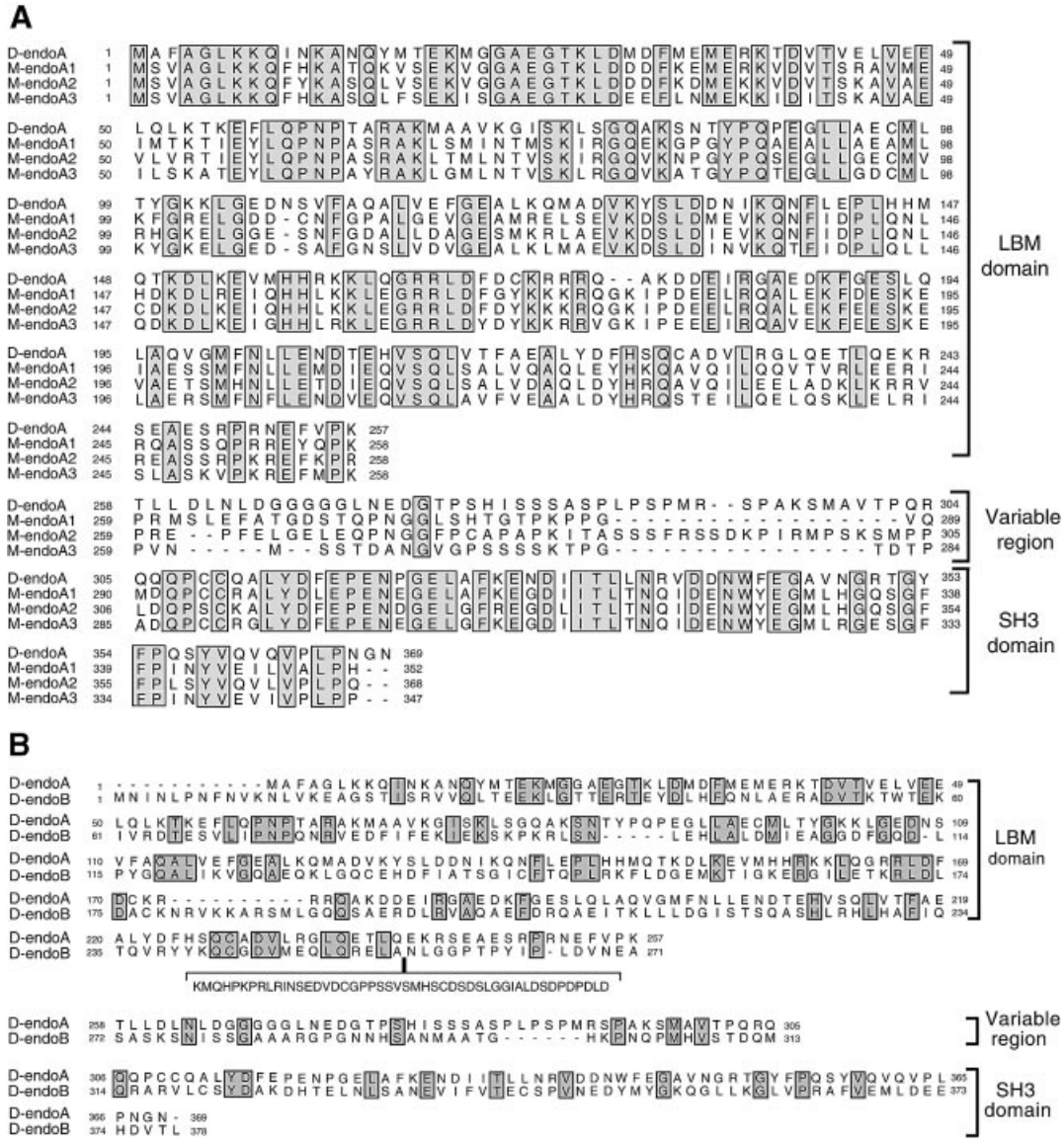

Fig. 1. *Drosophila* endophilins. (**A**) Sequence comparison between D-endoA and the murine endophilins (M-endo) A1, A2 and A3 (DDBJ/EMBL/GenBank accession Nos U58886, U58885 and U58887, respectively). The complete sequence of D-endoA was obtained from EST GH10390. The amino acid identity between D-endoA and mouse endophilins A1, A2 and A3 is 49, 51 and 52% respectively. (**B**) Sequence comparison between D-endoA and D-endoB. The complete sequence of D-endoB was obtained from EST LD42223; the corresponding mRNA is encoded by five exons and lacks the sequence encoded by exon 4 (see insertion; CG9834 in Flybase). The amino acid identity between D-endoA and D-endoB is 22%. In both (A) and (B), all sequences were aligned using Clustal_W. Residues identical between the aligned sequences are indicated by shaded boxes. The gene loci encoding D-endoA and D-endoB are referred to as FBgn0038659 and FBgn0034433 in Flybase (GadFly: CG14296 and CG9834).

terminals in the vicinity of, or in association with, SVs; and (iii) is recruited to sites of endocytosis.

Molecular and gross phenotypic characterization of mutants with deletions in the D-endoA gene

Using sequence information from the Berkeley *Drosophila* Genome Project (BDGP) database, we found a viable P-element insertion [EP(3)3502] in the *D-endoA* gene, located in the 3′–5′ orientation between nucleotides 105 and 106 of exon 1, which encodes most of the 5′-untranslated region (Figure 5A). We then generated 29 homozygous lethal alleles by imprecise excision of the P-element. Three of them (*endo*^{10}, *endo*^{21} and *endo*^{26}) did not complement *Df(3R)cha7*, which includes deletion of the *D-endoA* gene, and therefore were candidates to be mutations in the *D-endoA* gene. For *endo*^{10} and *endo*^{26}, the precise mutations were determined by sequencing of PCR fragments (Figure 5A).

endo^{10}, which contains 176 nucleotides of residual P-element (Figure 5A), is a partial loss-of-function allele, which causes a light loss of motility at the mature L3 larval stage and an extended L3 larval phase followed by larval lethality with a paralytic phenotype.

The deletion in *endo*^{26} includes loss of the entire LBM domain of D-endoA (Figure 5A). Homozygous *endo*^{26} causes lethality at the latest in second instar larvae, with a loss-of-motility phenotype. *Df(3R)cha7/endo*^{26} larvae showed the same mutant phenotype and lethality phase as *endo*^{26}*/endo*^{26} larvae, indicating that the phenotype and lethality of the latter were not due to possible additional mutations outside the genomic region missing in *Df(3R)cha7*. No D-endoA mRNA expression was detected

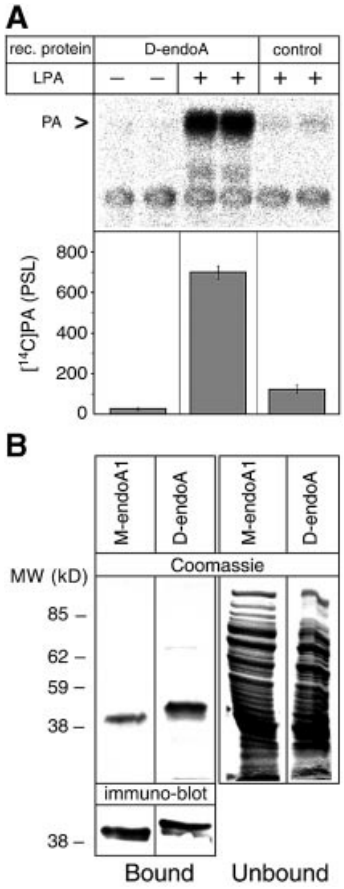

Fig. 2. D-endoA exhibits LPAAT activity and contains a functional SH3 domain. (**A**) Duplicate LPAAT assays using 10 μM [^{14}C]oleoyl-CoA and either purified recombinant (rec.) GST–D-endoA (50 μg/ml) or a virtually inactive purified GST mouse endophilin A1 fusion protein used as control (see Materials and methods, 25 μg/ml) were carried out in the absence (–) or presence (+) of 10 μM LPA as indicated. Top: autoradiogram; PA, phosphatidic acid. Bottom: quantitation of the [^{14}C]PA generated per equal amount of recombinant protein; bars indicate the variation of the duplicate values from the mean. (**B**) Binding of recombinant His-tagged mouse endophilin A1 (M-endoA1) and D-endoA to poly(L-proline)–Sepharose beads. Top: equal aliquots of the dimethylsulfoxide eluates from the poly(L-proline)–Sepharose beads (Bound) and the bead supernatant (Unbound) were analysed by SDS–PAGE and Coomassie Blue staining. Bottom: aliquots of poly(L-proline)–Sepharose beads (Bound) were analysed directly by SDS–PAGE followed by immunoblotting.

upon *in situ* hybridization of *endo*^{26}/*endo*^{26} embryos, indicating that *endo*^{26} represents a null allele (Figure 5B). In addition, no D-endoA maternal contribution could be detected, since *endo*^{26}/*endo*^{26} larvae showed the same mutant phenotype and lethality phase if they derived from *endo*^{26} germline clones.

endo^{21}, which consistently showed the same phenotype as *endo*^{26}, appeared to be a complete deletion of the D-endoA open reading frame (ORF) as well as flanking sequences (data not shown), and was not characterized further.

Because of the early lethality of *endo*^{26}/*endo*^{26} larvae, we were not able to analyse the NMJs in these D-endoA null mutants. We therefore focused on transheterozygous *endo*^{10}/*endo*^{26} mutants, which showed a stronger loss-of-motility phenotype than *endo*^{10}/*endo*^{10} mutants and lethality with paralysis during the L3 larval stage. In order to verify that this lethality is due to a defect in D-endoA expression, we used the UAS/Gal4 expression system to rescue the mutants. Indeed, when *endo*^{10}/*endo*^{26} larvae were induced for ubiquitous expression of D-endoA using *pUASp-D-endoA* under the control of *armadillo-Gal4* (*arm-Gal4*), flies developed into viable and fertile adults. This shows that D-endoA exerts an essential biological function. In contrast to the rescue of the *endo*^{10}/*endo*^{26} mutants, expression of D-endoA did not rescue the lethality of the *endo*^{10}/*endo*^{10} larvae (but appeared to improve the motility defects and did revert the alterations in presynaptic morphology, see Figure 10), indicating that an additional, essential locus had been affected by imprecise excision of the P-element.

Reduction of synaptic D-endoA levels impairs SV recycling

The above results prompted us to study the NMJs of *endo*^{10}/*endo*^{26} L3 larvae in greater detail. Double immunofluorescence analysis for D-endoA and CSP yielded three results. First, the presynaptic level of D-endoA in *endo*^{10}/*endo*^{26} larvae (Figure 4D and F) was drastically reduced compared with the wild type (Figure 4B), on average by 75% (see legend to Figure 4). We noticed that the levels of the D-endoA protein were very variable in different boutons within a single animal, suggesting that the levels of D-endoA in the nervous system fail to be regulated properly by the *endo*^{10} allele. Secondly, the localization of both CSP and D-endoA within the presynaptic terminals of *endo*^{10}/*endo*^{26} larvae was distinct from that of wild type, being shifted to the presynaptic plasma membrane and the cytoplasm beneath (Figure 4G and H). Thirdly, the overall structure of the NMJ was changed in that there was increased staining for CSP and D-endoA of the plasma membrane and the adjacent cytoplasm between the boutons. These observations suggested that massive reduction in the presynaptic D-endoA level impairs the SV cycle.

We used electrophysiology of L3 larvae NMJs to determine whether reduction in the presynaptic D-endoA level impairs SV exocytosis. No significant difference between *endo*^{10}/*endo*^{26} mutants and *endo*^{10}/+ heterozygous larvae used as controls could be observed with regard to mean mEJP frequency (Figure 6A), mEJP amplitude (Figure 6B) and mean quantal content of nerve-evoked EJPs upon 1 Hz stimulation (Figure 6C). This indicated that neurotransmitter release probability, and hence SV exocytosis, is not affected in the *endo*^{10}/*endo*^{26} mutants.

To study SV endocytosis in *endo*^{10}/*endo*^{26} mutants, we analysed FM1-43 internalization into NMJs of L3 larvae during electrophysiological stimulation (Ramaswami *et al*., 1994). In wild type (Figure 7B, top), consistent with the distribution of CSP in the presynaptic terminal (Figure 4A), the endocytosed membranes stained by the dye occupied large areas within the presynaptic bouton, as previously described (Ramaswami *et al*., 1994). In contrast, in *endo*^{10}/*endo*^{26} mutants, the FM1-43 staining was concentrated at the plasma membrane and the cytoplasm beneath (Figure 7B, bottom). The average FM1-43 uptake into >200 synaptic boutons during tetanic stimulation (30 Hz, 30 s) was reduced by >30% in *endo*^{10}/*endo*^{26}

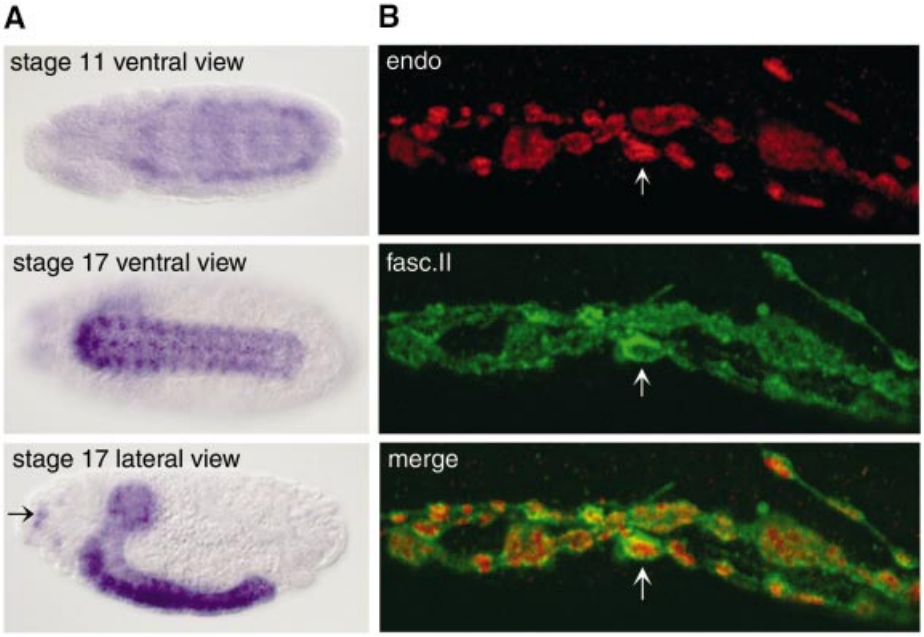

Fig. 3. Expression of D-endoA in the *Drosophila* nervous system. (**A**) *In situ* hybridization for the D-endoA mRNA at various stages of embryonic development. Note the strong staining in the CNS and in some ganglia of the peripheral nervous system such as the Bolwig organs (arrow). (**B**) Double immunofluorescence of D-endoA (endo, red) and fasciclin II (fasc.II, green) in the NMJs of L3 larvae. Note the staining for D-endoA inside the boutons and for fasciclin II at their periphery (arrows).

larvae compared with wild type (Figure 7A). SV exocytosis during tetanic stimulation for 30 s, as determined from the quantal content of evoked EJPs, was not reduced in $endo^{10}/endo^{26}$ mutants compared with $endo^{10}/+$ heterozygous larvae used as controls (data not shown). Hence, the decrease in FM1-43 uptake in the $endo^{10}/endo^{26}$ mutant was not due to unequal dye loading but, rather, reflected a reduction in the amount of SV membrane that was endocytosed.

We analysed the variability in the levels of FM1-43 uptake in both wild-type and $endo^{10}/endo^{26}$ mutant NMJs (Figure 7C). In wild type, the boutons with a low amount of dye uptake (<20 arbitrary fluorescence units) constituted only ~3% of all boutons (Figure 7C top, category 1). Consistent with the lower average FM1-43 uptake, ~40% of all boutons fell into this category in the $endo^{10}/endo^{26}$ mutants (Figure 7C, bottom, category 1), and the boutons with a high amount of dye uptake (>54 arbitrary fluorescence units), which represented ~15% of the total in wild type (Figure 7C, top, category 3), were rarely observed (<5% of total, Figure 7C, bottom, category 3). We conclude that D-endoA is required for efficient recycling of SVs from the plasma membrane.

Mutant D-endoA synapses largely devoid of SVs lack membrane budding intermediates whereas synapses still containing SVs show an increase in early-stage intermediates

Given these observations, we investigated the ultrastructure of the NMJs of L3 $endo^{10}/endo^{26}$ larvae by electron microscopy (EM). Consistent with the variability in the reduction of the D-endoA protein level in the $endo^{10}/endo^{26}$ mutant synapses, we observed a range of alterations as compared with the normal ultrastructure (Figure 8A). In ~30% of the synapses analysed, the presynaptic terminal was almost totally depleted of SVs (referred to as grade III depletion, Figure 8B). The few residual SVs were associated preferentially with the T-bar, i.e. the active zone (arrow in Figure 8B). Remarkably, the plasmalemma of these synapses did not show an obvious accumulation of budding intermediates with a significant degree of membrane curvature. However, in the majority of cases (~60% of the synapses), there was substantial (but not an almost total) depletion of SVs (grade II depletion), with the remaining SVs being concentrated at the active zone (an example is indicated by the arrow in Figure 8C). In ~10% of the synapses, there was no striking loss of SVs (grade I depletion, Figure 8F) but nonetheless an obvious change in ultrastructure, i.e. a remarkable increase in endocytic pits at the plasma membrane (arrowheads in Figure 8F). Interestingly, virtually all of these represented early-stage budding intermediates, i.e. shallow pits up to the hemispherical stage, rather than late-stage budding intermediates, i.e. deeply invaginated, constricted (near-spherical) pits. In grade I–III-depleted synapses, there was an increased incidence of vacuoles, which were often found in close proximity to the plasma membrane and in the vicinity of the active zone (Figure 8, asterisks in D and F, arrowheads in D and E). A quantitative analysis of the various synaptic boutons of $endo^{10}/endo^{26}$ larvae in comparison with wild type revealed that, on average, (i) the number of SVs was reduced by ~80% (Figure 10C, filled columns) and (ii) the occurrence of early-stage budding intermediates increased 3-fold (Figure 10C, open columns).

EM analysis of the NMJs of L3 $endo^{10}/endo^{10}$ larvae (Figure 9) showed, in the vast majority of cases, grade I (55% of synapses) and grade II (~40% of synapses)

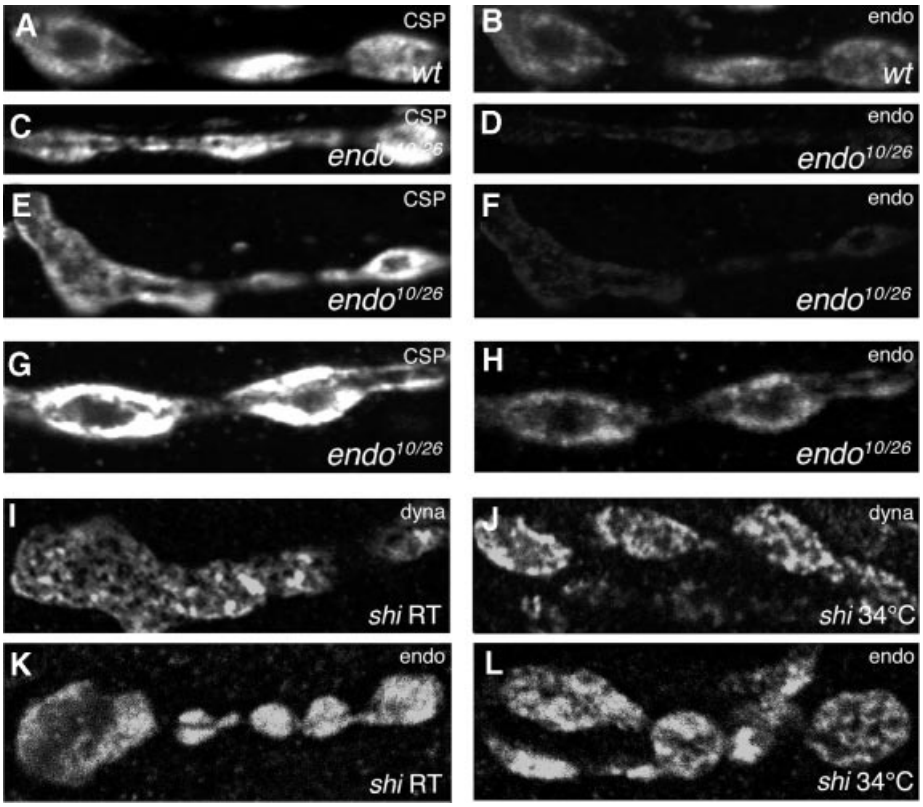

Fig. 4. Localization of D-endoA in the NMJ of wild-type and *endo*^{10}/*endo*^{26} L3 larvae. (**A**–**H**) Double immunofluorescence for CSP (left) and D-endoA (endo; right). (A and B) Wild type (wt). (C and D), (E and F) and (G and H) Three examples of *endo*^{10}/*endo*^{26} mutants (*endo*^{10}/^{26}). (A–F) Identical parameters of confocal microscopy for (A) versus (C) and (E), and for (B) versus (D) and (F). Note the decrease in D-endoA immunoreactivity in the *endo*^{10}/*endo*^{26} mutant [1.33 ± 0.68 (SD) arbitrary units, 30 boutons, three larvae] compared with wild type [5.22 ± 0.33 (SD) arbitrary units, 50 boutons, three larvae]. (G and H) The parameters of confocal microscopy were adjusted selectively to bring the signal of D-endoA immunostaining (H) up to a level similar to wild type. Note the shift in the subcellular localization of CSP and D-endoA from the presynaptic cytoplasm in wild type (A and B) to the plasma membrane and the cytoplasm beneath in the *endo*^{10}/*endo*^{26} mutant (C–G and H). (**I**–**L**) Localization of dynamin (dyna) and D-endoA (endo) in the NMJs of *shibire* L3 larvae. (I and K) NMJs in calcium-free saline at permissive temperature (room temperature, *shi* RT). (J and L) NMJs incubated for 5 min in calcium-containing high K^+ buffer at restrictive temperature (*shi* 34°C).

depletion of SVs. As in the grade I-depleted synapses of *endo*^{10}/*endo*^{26} larvae, there was a striking increase in early-stage, but not late-stage, budding intermediates at the plasma membrane adjacent to the active zone (Figure 9A–C, arrowheads). The curvature of these endocytic pits was less than that of the SVs. In addition, vacuolar structures were observed more frequently than in wild type (Figure 9). A quantitative analysis of the various synaptic boutons of *endo*^{10}/*endo*^{10} larvae in comparison with wild type revealed that, on average, (i) the number of SVs was reduced by more than half (Figure 10C, filled columns) and, remarkably, (ii) the occurrence of early-stage budding intermediates increased 6-fold (Figure 10C, open columns).

Expression of D-endoA from a transgene in L3 larvae reverted the alterations in NMJ ultrastructure for both *endo*^{10}/*endo*^{26} (Figure 10A) and *endo*^{10}/*endo*^{10} (Figure 10B) mutants (although it did not rescue the lethality of the latter). Specifically, the number of SVs approached the wild-type level (Figure 10C, filled columns) and the occurrence of endocytic pits fell even below that observed in wild-type NMJs (Figure 10C, open columns).

These ultrastructural observations allow us to draw three conclusions about the consequences of reducing presynaptic D-endoA levels. First, the SVs at the active zone are the most resistant to depletion upon lack of D-endoA. Secondly, massive reduction of presynaptic D-endoA, as indicated by an almost total depletion of SVs, does not lead to an accumulation of significantly curved budding intermediates. Thirdly, a less massive reduction of presynaptic D-endoA, which still allows SV recycling as indicated by the presence of a substantial number of SVs, increases the probability of capturing early-stage, but not late-stage, intermediates of the budding process upon fixation. Taken together, this indicates that D-endoA has a crucial role in SV endocytosis that becomes essential when the planar plasma membrane becomes curved, i.e. at the onset of budding.

Discussion

Our study of D-endoA hypomorphs, in particular of *endo*^{10}/*endo*^{26}, which is rescued by transgenic expression of D-endoA, shows that D-endoA becomes a vital component during the larval stage of the *Drosophila* life cycle. Given that loss of motility is the most striking phenotypic feature of larvae lacking D-endoA, the vital role of D-endoA is most likely in synaptic transmission, in particular at the NMJ where the protein is concentrated

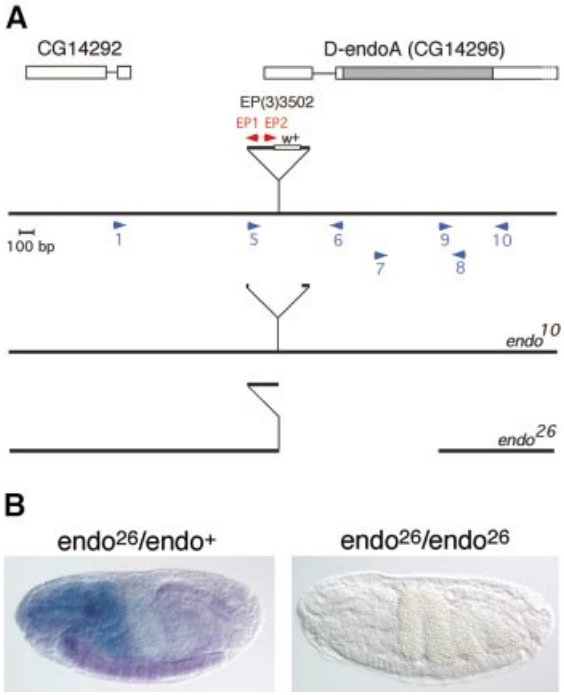

Fig. 5. Characterization of *D-endoA* mutant alleles. (**A**) Molecular characterization of *endo*^{10} and *endo*^{26}. The *D-endoA* gene contains at least two exons (boxes). Alignment of the nucleotide sequence of EST GH10390 with the genomic sequence of *D-endoA* (Flybase accession No. FBgn0038659, GadFly accession No. CG14296) revealed that the ORF of D-endoA is encoded by exon 2 only (grey box). The P-element, EP(3)3502, is inserted in the 3′–5′ orientation between nucleotides 105 and 106 of exon 1 and is not drawn to scale; w^{+}, *white* gene. Blue and red arrowheads indicate the position of some of the primers used for PCR amplification. For *endo*^{10}, sequencing of the PCR fragment obtained with primers 1 and 6 revealed deletion of most of the P-element, with a duplication of nucleotides 106–113 of exon 1 being followed by 13 nucleotides from the 3′-terminal repeat of the P-element, 163 nucleotides from its 5′ end, and nucleotides 106–113 of exon 1. For *endo*^{26}, sequencing of the two PCR fragments obtained with primers 1 and EP1 and with primers EP2 and 8 revealed deletion of (i) 5714 nucleotides from the 5′ end of the P-element; (ii) the exon 1 sequence 3′ to the transposon insertion site; (iii) intron 1; and (iv) the 5′ 814 nucleotides of exon 2; the duplicated nucleotides 106–113 of exon 1 are followed by the 3′ portion of the P-element, and nucleotide 2272 from its 3′ end is contiguous with the codon for Pro250 (see Figure 1A). Consistent with this, in *endo*^{26}, the region between primers 9 and 10 could be amplified and showed wild-type sequence whereas the regions between primers 5 and 6, and 7 and 8 could not be amplified. (**B**) *endo*^{26} is a null allele. Combined *in situ* hybridization for the D-endoA mRNA (entire ORF) (purple) and staining for β-galactosidase (blue) of stage 17 embryos. Left: heterozygous *endo*^{26} embryo, with the wild-type copy of D-endoA on a balancer chromosome expressing β-galactosidase under the control of the hunchback promoter (Tm3-*hbLacz*). β-galactosidase is expressed in the head region and D-endoA mRNA is detected in the ventral cord as in wild type. Right: homozygous *endo*^{26} embryo. Note the absence of both D-endoA mRNA and β-galactosidase activity.

presynaptically. The specific role of D-endoA in the presynaptic terminal is in a key step of the SV cycle, the endocytosis of the vesicle membrane from the plasmalemma, as will be discussed below. Our observations complement and extend previous observations on the role of endophilin A1 in vertebrates. These studies had shown that endophilin A1 is required for SLMV formation from the plasma membrane in a cell-free system (Schmidt and Huttner, 1998; Schmidt *et al*., 1999) and that interference

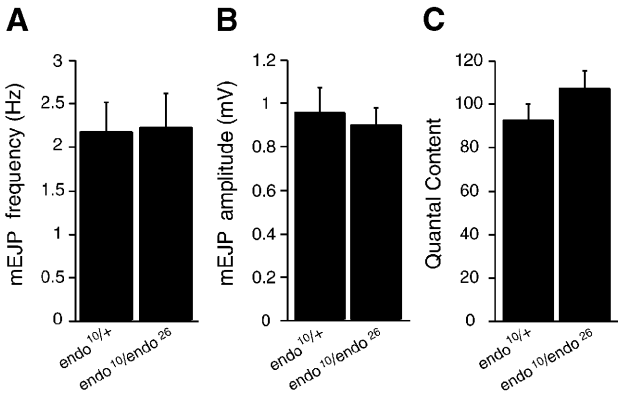

Fig. 6. Neurotransmitter release probability is not affected in *endo*^{10}/*endo*^{26} L3 larvae NMJs. (**A**) Mean mEJP frequency, (**B**) mean mEJP amplitude and (**C**) mean quantal content of nerve-evoked EJPs upon 1 Hz stimulation in *w;endo*^{10}/*endo*^{26} (n = 7) and their siblings *w;endo*^{10}/+ (n = 5). Bars indicate SEM.

with the SH3 domain of endophilin A blocks SV endocytosis in a living synapse (Ringstad *et al*., 1999; Gad *et al*., 2000).

Given these observations in the vertebrate model systems, why is there still some motility, indicative of residual synaptic transmission and hence of residual levels of SVs, in the D-endoA null mutant *endo*^{26}/*endo*^{26}? One possible explanation is that the second *Drosophila* endophilin, D-endoB, is also expressed in neurones and can substitute functionally for the lack of D-endoA during embryonic and larval stages. Another is that there is a pathway of SV recycling, for example by 'kiss-and-run' (Hannah *et al*., 1999; Valtorta *et al*., 2001), that does not require D-endoA and that provides a level of SVs sufficient for life during embryonic and larval stages. A third possibility is that D-endoA is essential for SV endocytosis only in mature synapses, whereas early in development the complete lack of D-endoA only severely impairs this process, possibly because the efficiency of recycling needs to be increased at later developmental stages, or some mechanistic aspect of the process changes during development.

In the wild-type NMJ, D-endoA was found to be localized in the presynaptic cytoplasm in a pattern consistent with it being present in close proximity to, or even in (transient) association with, the membrane of SVs. In contrast, in the hypomorph NMJs of *endo*^{10}/*endo*^{26} transheterozygous L3 larvae, the residual D-endoA in these mutants was observed predominantly in apparent association with the presynaptic plasma membrane and in the cytoplasm beneath. This is consistent with the residual D-endoA being recruited to the sites of SV endocytosis. A similar recruitment of D-endoA, albeit at wild-type level, was observed in *shibire* L3 larvae at the restrictive temperature, i.e. when SV exocytosis had been stimulated by depolarization but endocytosis was blocked due to dynamin dysfunction (Sever *et al*., 2000). Hence, in line with previous *in vitro* observations using synaptic membranes (Ringstad *et al*., 1999), conditions of defective SV endocytosis, be they due to lack of D-endoA or to dynamin dysfunction, reveal the recruitment of endophilin A to endocytotic sites.

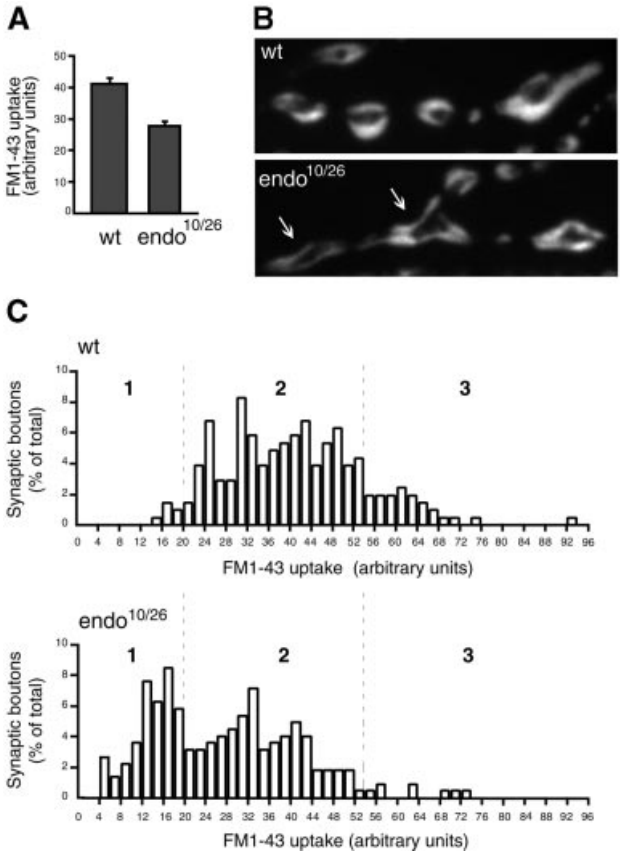

Fig. 7. FM1-43 uptake at the NMJs of wild-type and *endo*^{10}/*endo*^{26} L3 larvae. FM1-43 uptake was performed for 30 s under 30 Hz stimulation. (**A**) Average FM1-43 uptake into 206 wild-type (wt) and 223 *endo*^{10}/*endo*^{26} (*endo*$^{10/26}$) synaptic boutons. The arbitrary units are the MetaView brightness values × 10^{-1}. Bars indicate SEM; $P < 0.0001$. (**B**) Fluorescence pattern of endocytosed FM1-43 in wild-type (wt) and *endo*^{10}/*endo*^{26} (*endo*$^{10/26}$) NMJs. Note the shift in the FM1-43 staining from the presynaptic cytoplasm in wild type to the plasma membrane and cytoplasm beneath in the *endo*^{10}/*endo*^{26} mutant (arrows). The size of the FM1-43-stained boutons in the *endo*^{10}/*endo*^{26} mutant ($n = 41$) was found to be increased, on average, by 35% compared with wild type ($n = 77$). (**C**) Frequency of occurrence of synaptic boutons with various levels of FM1-43 uptake. The 206 wild-type (wt, top) and 223 *endo*^{10}/*endo*^{26} (*endo*$^{10/26}$, bottom) synaptic boutons were divided into groups according to the amounts of endocytosed FM1-43 (steps of two arbitrary units of fluorescence, abscissa), and the number of synaptic boutons in each group is expressed as a percentage of their total number (ordinate).

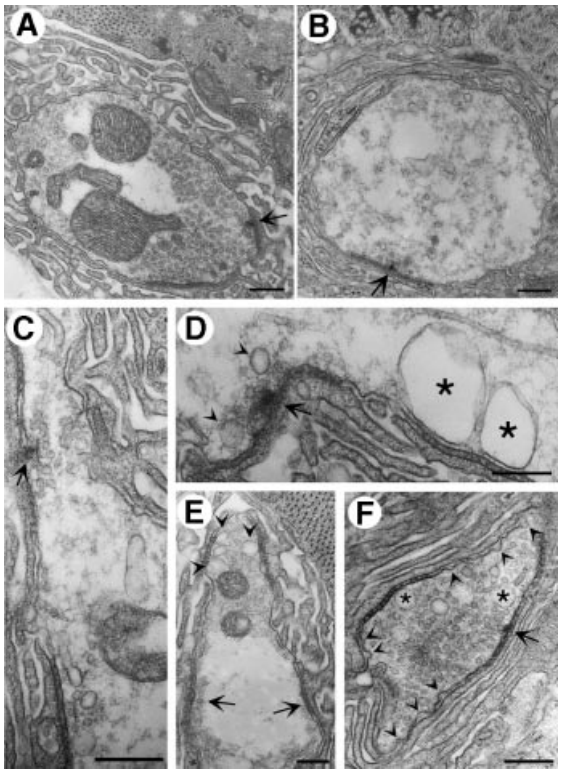

Fig. 8. Ultrastructural analysis of the NMJs of *endo*^{10}/*endo*^{26} L3 larvae. (**A**) Wild type. (**B**) An *endo*^{10}/*endo*^{26} NMJ almost completely devoid of SVs (grade III depletion). Note the few SVs remaining at the active zone (arrow). (**C**) An *endo*^{10}/*endo*^{26} NMJ with some residual SVs (grade II depletion), which are mostly clustered at the active zone (arrow). Note the pleiomorphic vesicles which are larger than SVs. (**D**) An *endo*^{10}/*endo*^{26} NMJ with a massively reduced pool of SVs (grade III depletion), showing large vacuoles in close proximity to the presynaptic membrane (asterisks). Note the vesicles which are larger than SVs near the active zone (arrowheads). Arrow, active zone. (**E**) An *endo*^{10}/*endo*^{26} NMJ in which SVs are lacking in some regions of the terminal-containing active zones (grade III depletion, arrows), whereas a reduced pool of SVs (grade I depletion) and pleiomorphic vesicular structures are found in other regions (arrowheads). (**F**) An *endo*^{10}/*endo*^{26} NMJ with an almost normal pool of SVs (grade I depletion), showing an increased incidence of shallow pits of the presynaptic membrane (arrowheads) as well as a few vacuoles (asterisks). Arrow, active zone. Upon analysis of the T-bar region of EM sections of 26 randomly chosen *endo*^{10}/*endo*^{26} NMJs, 31% showed grade III depletion as illustrated in (B), 58% showed grade II depletion as illustrated in (C), and 11% showed grade I depletion as illustrated in (F). All scale bars correspond to 500 nm.

At which stage in SV endocytosis does endophilin A act? Previous studies on the ultrastructure of the lamprey giant synapse under conditions of acute interference with the SH3 domain of endophilin A resulted in the depletion of SVs, caused by blocking the later stages of the endocytic process, i.e. the transition of shallow to deeply invaginated, constricted coated pits (Ringstad *et al*., 1999), and fission (Gad *et al*., 2000). In contrast, in those hypomorph NMJs of *endo*^{10}/*endo*^{26} transheterozygous L3 larvae that were virtually devoid of SVs (grade III depletion), there was no striking increase in shallow or deeply invaginated plasmalemmal pits. In other words, whereas the interference with the SH3 domain of endophilin A still allows membrane budding to proceed, depending on the mode of interference, to the hemispherical stage (Ringstad *et al*., 1999) or even the near-spherical stage (Gad *et al*., 2000), in the absence of endophilin A or upon its massive reduction there appears to be little, if any, budding of the SV membrane from the planar plasmalemma, despite the abundant presence of SV membrane constituents in the plasma membrane and of the clathrin coat machinery in the cytosol. Bearing in mind that, in contrast to the acute manipulation of endophilin A in the lamprey giant synapse (Ringstad *et al*., 1999; Gad *et al*., 2000), the deprivation of endophilin A at the NMJ of the mutant larvae is a chronic situation, it is conceivable that membrane buds formed transiently in the absence of endophilin A but reverted to a planar shape over time. However, our data raise the possibility that the function of endophilin A in SV membrane budding is so critical, and sets in so early in the budding process, that once the level of endophilin A has fallen below a threshold level, even

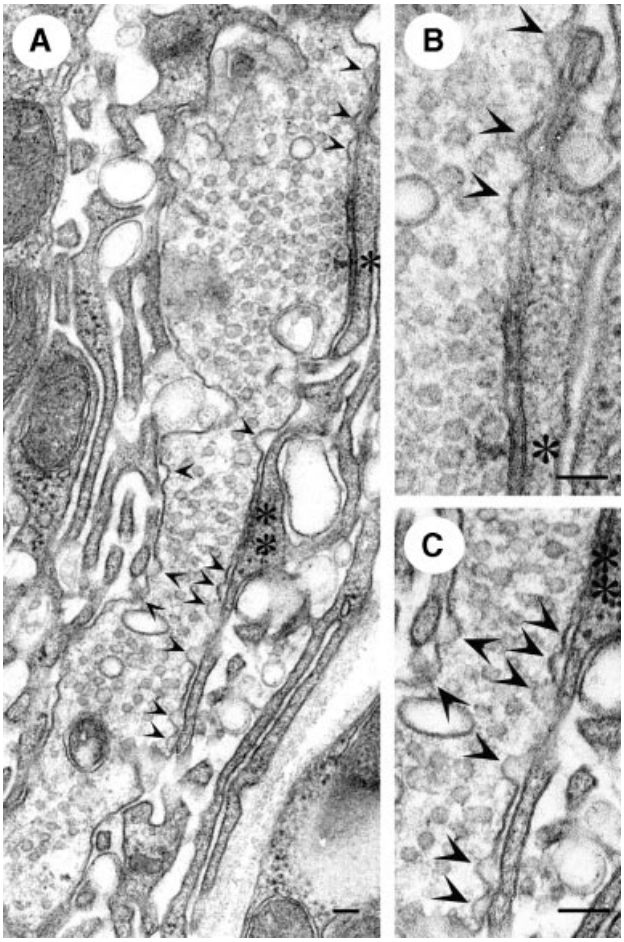

Fig. 9. Ultrastructural analysis of the NMJ of *endo*^{10}/*endo*^{10} L3 larvae. (**A**) A grade I-depleted *endo*^{10}/*endo*^{10} NMJ with an almost normal pool of SVs and a striking increase in shallow pits of the presynaptic membrane (arrowheads). Two active zones are indicated by single and double asterisks, respectively. (**B** and **C**) Magnification of the active zones indicated in (A) by the single asterisk (B) and by the double asterisk (C). Note the numerous shallow pits of the presynaptic membrane near the active zone (arrowheads). Upon analysis of the T-bar region of EM sections of 19 randomly chosen *endo*^{10}/*endo*^{10} NMJs, 55% showed grade I depletion as illustrated in (A), 39% showed grade II depletion (not illustrated), and 6% showed grade III depletion (not illustrated). Scale bars correspond to 100 nm in (A), 115 nm in (B) and 150 nm in (C).

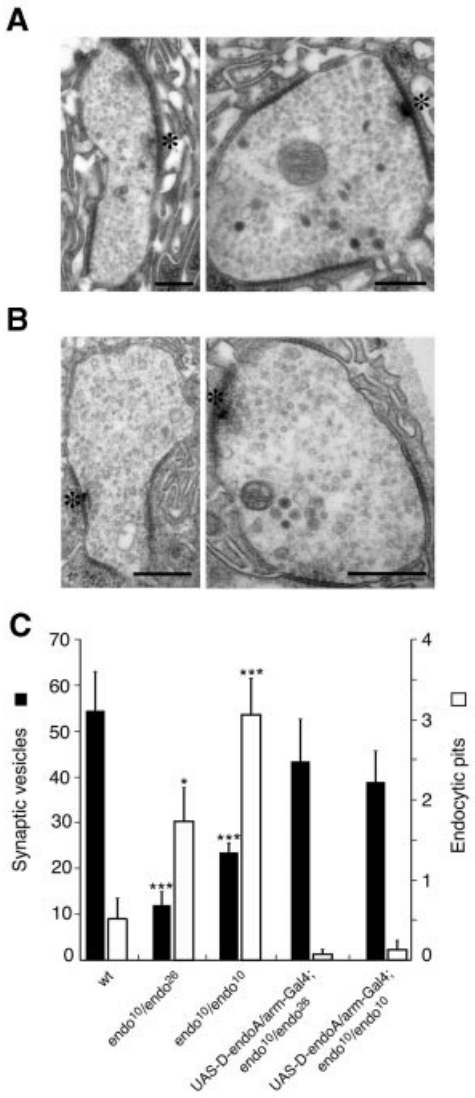

Fig. 10. Ultrastructural analysis of the NMJs of *pUASp-D-endoA/arm-Gal4*; *endo*^{10}/*endo*^{26} and *pUASp-D-endoA/arm-Gal4*; *endo*^{10}/*endo*^{10} L3 larvae. (**A**) Two examples of NMJs of *pUASp-D-endoA/arm-Gal4*; *endo*^{10}/*endo*^{26} L3 larvae. (**B**) Two examples of NMJs of *pUASp-D-endoA/arm-Gal4*; *endo*^{10}/*endo*^{10} L3 larvae. (A and B) Asterisks, active zones. All scale bars correspond to 400 nm. (**C**) Quantitation of the number of SVs at, and nearby, the active zone (filled columns) and of the number of endocytic pits adjacent to the active zone (open columns) per section in NMJs of wild-type (wt, 15 boutons, three larvae), *endo*^{10}/*endo*^{26} (26 boutons, three larvae), *endo*^{10}/*endo*^{10} (19 boutons, three larvae), *pUASp-D-endoA/arm-Gal4*; *endo*^{10}/*endo*^{26} (16 boutons, two larvae) and *pUASp-D-endoA/arm-Gal4*; *endo*^{10}/*endo*^{10} (10 boutons, two larvae) L3 larvae. Bars indicate SEM. Values with a statistically significant difference from wild type are indicated by asterisks; $*P < 0.05$; $***P < 0.0005$.

shallow pits of the plasma membrane can no longer form. The increased incidence of shallow plasmalemmal pits in the hypomorph NMJs of *endo*^{10}/*endo*^{10} homozygous L3 larvae and in the mildly affected (grade I-depleted) NMJs of *endo*^{10}/*endo*^{26} transheterozygous L3 larvae would be consistent with this possibility, if one assumes that the nearly normal number of SVs in these NMJs was indicative of a reduced endophilin A level that, however, was still above this threshold.

The plasmalemmal pits in the NMJs of *endo*^{10}/*endo*^{10} homozygous L3 larvae and in the grade I-depleted NMJs of *endo*^{10}/*endo*^{26} transheterozygous L3 larvae are reminiscent of the shallow coated pits observed in stimulated lamprey giant synapses upon microinjection of antibody to the SH3 domain of endophilin A (Ringstad *et al*., 1999). However, aside from the differences in experimental approach, there is a key difference between the latter study and the present work concerning the significance of these hemispherical pits. In the case of the antibody microinjection into the lamprey giant synapse (Ringstad *et al*., 1999), SVs became depleted, and hence these pits were indicative of the membrane budding process proceeding through the early stages (up to the hemispherical pit) but being blocked thereafter (thus the lack of late-stage budding intermediates, i.e. the deeply invaginated, constricted or near-spherical pit). In contrast, in the case of the reduced D-endoA levels in the hypomorph NMJs of the mutant larvae, the early-stage budding intermediates were seen

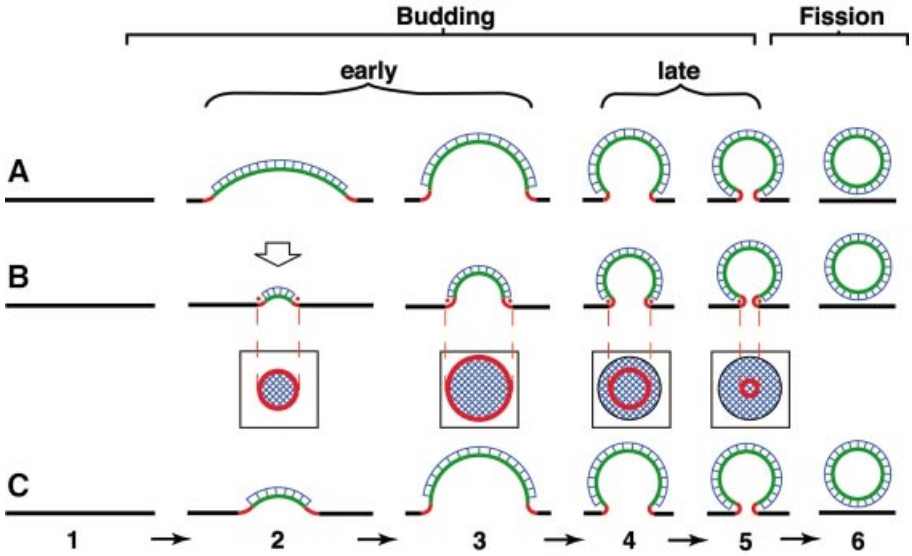

Fig. 11. Three models for the budding of the SV membrane from the presynaptic plasma membrane. Intermediates in the budding process are indicated by numbers; 1, planar plasma membrane; 2 and 3, early intermediates, i.e. shallow coated pits; 3, hemispherical pit; 4 and 5, late intermediates; 5, deeply invaginated, constricted or near-spherical pit; 6, endocytic/SV after fission and prior to uncoating. Black, planar membrane (zero curvature); green, membrane of the bud proper (positive curvature); red, membrane at the edge of the bud (mixed positive–negative curvature, see Figure 8 in Schmidt *et al*., 1999); blue, clathrin coat. The dynamin ring around the neck of the deeply invaginated, constricted, near-spherical pit (intermediate 5) is not shown for clarity. (**A**) Budding via a continuous increase in the curvature of a constant membrane area which corresponds to the surface of the future vesicle ('making-a-fist' model). (**B**) Budding via a continuous increase in the area of curved membrane, with the curvature of the membrane bud being constant irrespective of the size of the bud ('rising-sun' model). The square boxes indicate the circular configuration of the edge of the bud at various stages of the budding process, as it would appear in a view indicated by the open arrow above intermediate 2. Note that the circumference of the edge, and hence the amount of a molecule recruited to the edge (red dots), increases during the early stages of budding but decreases during the late stages. (**C**) Budding via the 'rising-sun' model during the early stages and via the 'making-a-fist' model during the late stages. Note that both the area of positively curved membrane constituting the bud proper (green) and the circumference of the edge of the bud (red) increase only during the early, but not the late, stages of budding.

predominantly in grade I-depleted synapses, i.e. those in which a nearly normal level of SVs was maintained. Hence, in the latter case, these pits are indicative of a slowing down of membrane budding specifically during the early stages, i.e. up to the hemispherical pit, without a block of the late stages (which still must have taken place, as did fission, given the nearly normal level of SVs).

Why would reduction of endophilin A slow down the early stages of membrane budding? There are two principal models for the budding of clathrin-coated vesicles, which have different implications for the membrane curvature changes that occur during budding (Kirchhausen, 2000; Wu *et al*., 2001). In one model, referred to as the 'making-a-fist' model (Figure 11A), there is a continuous increase in the curvature of a given membrane area (corresponding to the surface of the future vesicle) from zero (planar plasma membrane) to that of the final vesicle (Figure 11). In the other model, referred to as the 'rising-sun' model (Figure 11B), there is a continuous increase in the area of curved membrane, with the curvature of the membrane bud being constant irrespective of the size of the bud. Implicit in the latter model is that the amount of a protein recruited selectively to the edge of the bud (Figure 11B, red dots), which has a circular configuration, would increase only during the early, but not the late, stages of budding (Figure 11B, squared boxes, red ring).

Irrespective of which of these models is better compatible with steric considerations concerning the clathrin coat (Kirchhausen, 2000; Wu *et al*., 2001), it appears that neither explains the available morphological evidence concerning the size and shape of the pits of the presynaptic plasma membrane. It should be noted that the shallow coated pits observed in the present study as well as those accumulating upon anti-endophilin A antibody microinjection into the lamprey giant synapse (Ringstad *et al*., 1999) are larger, and hence have a lesser curvature, than SVs, whereas the deeply invaginated, constricted coated pits accumulating upon microinjection of the SH3 domain of endophilin A have a size and curvature very similar, if not identical to those of SVs (Gad *et al*., 2000). On the other hand, comparison of the various shallow pits observed in the present study and previously in the lamprey (Ringstad *et al*., 1999) does not reveal an obvious increase in curvature as budding proceeds to the hemispherical pit, as would be predicted from the 'making-a-fist' model (Figure 11A), but rather suggests a relatively constant curvature irrespective of the size of the shallow pit, consistent with the 'rising-sun' model (Figure 11B). In other words, the available morphological evidence on the budding of the SV membrane from the plasma membrane is best explained by the early stages occurring according to the 'rising-sun' model and the late stages according to the 'making-a-fist' model (Figure 11C). Interestingly, this would explain why a reduction of endophilin A would slow down in particular the early stages of membrane budding: the amount of endophilin A recruited to the developing bud would increase only during the early, but

not the late, stages of budding, irrespective of whether recruitment is to the edge of the bud (Figure 11C, red) or to the bud proper (Figure 11C, green).

The present data are consistent with the notion that endophilin A changes membrane curvature by its action on lipids. This notion, which originated from the observation that mammalian endophilin A1 exhibits intrinsic LPAAT activity and hence can alter the shape of membrane lipids (Schmidt *et al*., 1999), has received experimental support from a very recent report, describing the effects of recombinant endophilin A1 on liposomes (Farsad *et al*., 2001; Huttner and Schmidt, 2002). With regard to the specific changes in membrane curvature that occur during budding at the edge of the bud versus the bud proper, the exact roles of the LPAAT activity of endophilin A and its LBM domain remain to be determined. Via its LPAAT activity, which would reduce positive curvature if LPA is in the cytoplasmic membrane leaflet and acyl-CoA in the cytosol, endophilin A may contribute to the special membrane curvature at the edge of the bud if recruited to this site (Schmidt *et al*., 1999) (Figure 11, red). If, however, endophilin A condenses cytosolic LPA and acyl-CoA to PA and mediates membrane insertion of this phospholipid (Huttner and Schmidt, 2000), this would generate positive curvature, which may be a means by which endophilin A contributes to formation of the bud proper (Figure 11, green). The conversion of liposomes into narrow tubules by endophilin A, which was reported to be mediated by its LBM domain but to be independent of its LPAAT activity (Farsad *et al*., 2001; Huttner and Schmidt, 2002), demonstrates its ability to generate positive curvature, but it is presently unclear how this relates to the curvature changes of the bud proper versus the edge of the bud.

It should be stressed that the requirement for endophilin A throughout the budding process, starting at its initiation, which we believe is revealed by our study, does not contradict the proposed requirement for endophilin A in fission (Schmidt *et al*., 1999), as this has been established and shown to reflect a critical protein–protein interaction of endophilin's SH3 domain, most probably with dynamin (Gad *et al*., 2000). The crucial role of endophilin A as a bifunctional protein in SV endocytosis, acting on lipids as well as proteins, is also underscored by the conservation of its LBM domain and SH3 domain between vertebrates and invertebrates.

Materials and methods

Drosophila genetics

Generation of *D-endoA* mutants, molecular characterization of *endo*^{10} and *endo*^{26}, and transgenic expression of D-endoA was performed according to established procedures. For details, see Supplementary data.

Whole-mount in situ hybridization

The *D-endoA* transcript was detected by *in situ* hybridization using a digoxigenin-labelled antisense RNA probe obtained from the expressed sequence tag (EST) GH10390 (BDGP).

Immunocytochemistry

Immunocytochemistry of type 1b boutons was performed according to standard procedures. The peptide H_2N-CKRSEAESRPRNEFVP-$CONH_2$ was used to raise and affinity-purify the D-endoA antibody. When L3 larvae homozygous for the *shi*^{ts1} allele were used, the unfixed flat body muscle preparations were either rinsed with calcium-free saline at room temperature and fixed (control condition at the permissive temperature), or incubated for 5 min at 34°C (restrictive temperature) with a buffer containing 90 mM KCl followed by fixation. For details, see Supplementary data.

Electrophysiology

Electrophysiological analysis was performed according to established procedures as detailed in the Supplementary data.

FM1-43 uptake

FM1-43 uptake was performed as described (Ramaswami *et al*., 1994) with minor modifications (for details, see Supplementary data). Quantitative measurements were made of type 1b boutons of NMJ 6/7 that were in focus, measuring the average intensity in each bouton using MetaView (12 bits brightness value: 0-4096; exposure time 0.1 s). Background fluorescence of the muscle near the bouton was subtracted. The resulting MetaView brightness values were divided by 10 to yield the arbitrary units shown in Figure 7A and C.

Electron microscopy

Standard procedures of EM were used (for details, see Supplementary data). Quantitative analyses (see Figure 10C) of EM sections of randomly chosen presynaptic terminals showing one or more T-bars were performed as follows. SVs were counted within a square area of presynaptic cytoplasm of which one edge coincided with the active zone as defined by the electron-dense segment of the presynaptic plasma membrane, with the T-bar in the middle. For wild type, the mean number of SVs in this area was found to be 55. Three grades of depletion of SVs in this area were defined: grade I, 23–49 SVs (mean = 33); grade II, 7–22 SVs (mean = 11); grade III, 0–6 SVs (mean = 3.5). Endocytic pits of the presynaptic plasma membrane were counted on both sides of an active zone (identified by a T-bar).

Expression of recombinant D-endoA, LPAAT assay and poly(L-proline)–Sepharose binding

Bacterial expression and purification of a GST–D-endoA fusion protein and determination of its LPAAT activity followed previously described procedures (Schmidt *et al*., 1999). A GST mouse endophilin A1 fusion protein (GST–M-endoA1) served as negative control because, under the present experimental conditions, M-endoA1 fused at its N-terminus to GST was found to exhibit very low LPAAT activity as compared with M-endoA1 carrying an N-terminal His tag (data not shown). Poly(L-proline)–Sepharose binding of His_6-tagged D-endoA and mouse endophilin A1 was performed as described (Schmidt *et al*., 1999). For details, see Supplementary data. The nucleotide sequence data reported in this paper for D-endoA and D-endoB have been submitted to the DDBJ/EMBL/GenBank Database and have been assigned the accession numbers AJ437141 and AJ437142, respectively.

Supplementary data

Supplementary data for this paper are available at *The EMBO Journal* Online.

Acknowledgements

We thank S.Roth for supporting the work of A.G., U.Weiss for technical assistance, and K.Margitudis for artwork. A.G. was supported by a long-term EMBO fellowship, W.B.H. by grants from the DFG (SPP GTPases, Hu 275/5-1), the EC (ERB-FMRX-CT96-0023), the German–Israeli Foundation for Scientific Research and Development, and the Fonds der Chemischen Industrie, and A.A.S. by the ATIPE programme of the Centre National de la Recherche Scientifique and a grant from the Fondation pour la Recherche Médicale.

References

Estes,P.S., Roos,J., van der Bliek,A., Kelly,R.B., Krishnan,K.S. and Ramaswami,M. (1996) Traffic of dynamin within individual *Drosophila* synaptic boutons relative to compartment-specific markers. *J. Neurosci.*, **16**, 5443–5456.

Farsad,K., Ringstad,N., Takei,K., Floyd,S.R., Rose,K. and De Camilli,P. (2001) Generation of high curvature membranes mediated by direct endophilin bilayer interactions. *J. Cell Biol.*, **155**, 193–200.

Gad,H. *et al*. (2000) Fission and uncoating of synaptic clathrin-coated

vesicles are perturbed by disruption of interactions with the SH3 domain of endophilin. *Neuron*, **27**, 301–312.
González-Gaitán,M. and Jäckle,H. (1997) Role of *Drosophila* α-adaptin in presynaptic vesicle recycling. *Cell*, **88**, 767–776.
Hannah,M.J., Schmidt,A.A. and Huttner,W.B. (1999) Synaptic vesicle biogenesis. *Annu. Rev. Cell Dev. Biol.*, **15**, 733–798.
Huttner,W.B. and Schmidt,A. (2000) Lipids, lipid modification and lipid–protein interaction in membrane budding and fission—insights from the roles of endophilin A1 and synaptophysin in synaptic vesicle endocytosis. *Curr. Opin. Neurobiol.*, **10**, 543–551.
Huttner,W.B. and Schmidt,A. (2002) Membrane curvature: a case of endofeelin'…. *Trends Cell Biol.*, **12**, 155–158.
Kirchhausen,T. (2000) Clathrin. *Annu. Rev. Biochem.*, **69**, 699–727.
Micheva,K.D., Ramjaun,A.R., Kay,B.K. and McPherson,P.S. (1997) SH3 domain-dependent interactions of endophilin with amphiphysin. *FEBS Lett.*, **414**, 308–312.
Ramaswami,M., Krishnan,K.S. and Kelly,R.B. (1994) Intermediates in synaptic vesicle recycling revealed by optical imaging of *Drosophila* neuromuscular junctions. *Neuron*, **13**, 363–375.
Ringstad,N., Nemoto,Y. and De Camilli,P. (1997) The SH3p4/SH3p8/SH3p13 protein family: binding partners for synaptojanin and dynamin via a Grb2-like Src homology 3 domain. *Proc. Natl Acad. Sci. USA*, **94**, 8569–8574.
Ringstad,N., Gad,H., Löw,P., Di Paolo,G., Brodin,L., Shupliakov,O. and De Camilli,P. (1999) Endophilin/SH3p4 is required for the transition from early to late stages in clathrin-mediated synaptic vesicle endocytosis. *Neuron*, **24**, 143–154.
Schmidt,A. and Huttner,W.B. (1998) Biogenesis of synaptic-like microvesicles in perforated PC12 cells. *Methods*, **16**, 160–169.
Schmidt,A., Wolde,M., Thiele,C., Fest,W., Kratzin,H., Podtelejnikov,A.V., Witke,W., Huttner,W.B. and Söling,H.-D. (1999) Endophilin I mediates synaptic vesicle formation by transfer of arachidonate to lysophosphatidic acid. *Nature*, **401**, 133–141.
Sever,S., Damke,H. and Schmid,S.L. (2000) Garrotes, springs, ratchets and whips: putting dynamin models to the test. *Traffic*, **1**, 385–392.
Simpson,F., Hussain,N.K., Qualmann,B., Kelly,R.B., Kay,B.K., McPherson,P.S. and Schmid,S.L. (1999) SH3-domain-containing proteins function at distinct steps in clathrin-coated vesicle formation. *Nature Cell Biol.*, **1**, 119–124.
Slepnev,V.I. and De Camilli,P. (2000) Accessory factors in clathrin-dependent synaptic vesicle endocytosis. *Nature Rev.*, **1**, 161–172.
Valtorta,F., Meldolesi,J. and Fesce,R. (2001) Synaptic vesicles: is kissing a matter of competence? *Trends Cell Biol.*, **11**, 324–328.
Wu,X., Zhao,X., Baylor,L., Kaushal,S., Eisenberg,E. and Greene,L.E. (2001) Clathrin exchange during clathrin-mediated endocytosis. *J. Cell Biol.*, **155**, 291–300.

Received October 31, 2001; revised and accepted February 21, 2002

Note added in proof

Verstreken *et al*. (*Cell*, April 2002) have independently isolated *Drosophila* endophilin A mutants and shown that endophilin A is essential for synaptic vesicle endocytosis.